ChemSusChem

Research Article
doi.org/10.1002/cssc.202501775

Chemistry Europe
European Chemical Societies Publishing

www.chemsuschem.org

The Key to Enzymatic Degradation of Polybutylene Terephthalate (PBT): Influence of Semicrystalline Properties on Degradation

Annalena Pongratz, Andreas Gagsteiger, Birte Höcker,* and Holger Ruckdäschel*

The rapidly growing plastic production and its environmental impact necessitate closed-loop recycling strategies for all polymers. For polyesters, which are susceptible to hydrolysis, enzymatic degradation offers a promising solution. While amorphous polyethylene terephthalate (PET) is already fully degradable, enzymatic breakdown of polybutylene terephthalate (PBT) remains challenging and underexplored. This study investigates the enzymatic degradability of PBT by systematically modifying its semicrystalline structure and optimizing enzymatic degradation conditions. Several PET-hydrolases were tested for their capability to degrade PBT, with LCC variants proving most effective. Increasing incubation temperatures drastically improve the release of soluble degradation products of PBT, with 80 °C as optimum. To assess the impact of semicrystalline properties, PBT substrates with varying contents of mobile amorphous fraction (MAF), rigid amorphous fraction (RAF), and crystalline fractions, as well as different lamellar morphologies, are prepared. Degradation trials reveal that lowering crystallinity significantly improve enzymatic PBT hydrolysis, yielding up to 1.7 mM of soluble products within 24 h. Both MAF and RAF are hydrolyzed at comparable rates, whereby incubation temperatures near the glass transition of RAF are required for significant hydrolysis. These findings demonstrate the interplay between material and enzyme properties, showcasing that fine-tuning both is key to advancing efficient enzymatic PBT recycling.

1. Introduction

The consumption of plastic products has grown continuously since the start of their industrial production over a century ago. In 2022 alone, over 400 million metric tons of plastic products were produced.[1,2] This growth, coupled with missing or inadequate end-of-life management and the use of mainly crude oil for production, has led to significant environmental problems. In response, governments worldwide are attempting to counteract these developments by implementing recycling targets and restrictions. These target both commodity plastics, particularly in packaging, as well as engineering plastics, such as those used in the automotive industry.[3,4]

To meet the political restrictions and to reduce the environmental impact of plastic products, several recycling strategies are investigated. Among these, mechanical, chemical, and biological recycling have gained academic and industrial attention. Biological recycling, specifically enzymatic hydrolysis, is particularly promising. It could allow selective, closed-loop recycling from mixed plastic waste under mild conditions and without harsh chemicals.[5,6]

Semiaromatic polyesters such as polyethylene terephthalate (PET) and polybutylene terephthalate (PBT) are of particular interest for closed-loop recycling due to their widespread use in the packaging, automotive, and electrical industries.[7–9] Both polyesters are semicrystalline and challenging substrates for enzymatic degradation. Their morphology is best described using the three-phase model, which differentiates between crystalline regions X_c and an amorphous phase that is subdivided into two distinct sub-phases: the mobile amorphous phase (MAF) and the rigid amorphous phase (RAF). Compared to the crystalline domains, both amorphous phases exhibit lower chain packing density and reduced molecular orientation. The RAF primarily serves as a transitional layer between the crystalline structures and MAF. Within the RAF, chain segments are subject to mobility restrictions as a result of their proximity to and interaction with the crystalline phase.[10,11] Because of these constraints, RAF does not devitrify at the glass transition temperature (T_g) of MAF; instead, its T_g is shifted to higher temperatures ≈101 °C for PBT, and 200 °C for PET.[12–14] The proportions of crystalline, RAF, and MAF phases are influenced by the polymer type and its thermal history.[10,13,14] PET, characterized by slower crystallization kinetics compared to PBT,[10,15] typically exhibits low crystallinity levels even in commercial applications. In contrast, commercial PBT generally has a crystallinity degree above 40%, depending

A. Pongratz, H. Ruckdäschel
Department of Polymer Engineering
University of Bayreuth
Universitätsstrasse 30, 95447 Bayreuth, Germany
E-mail: holger.ruckdaeschel@uni-bayreuth.de

A. Gagsteiger, B. Höcker
Department of Biochemistry
University of Bayreuth
Universitätsstrasse 30, 95447 Bayreuth, Germany
E-mail: birte.hoecker@uni-bayreuth.de

Supporting information for this article is available on the WWW under https://doi.org/10.1002/cssc.202501775

on production methods and grade.[16] Under conventional processing, amorphous and crystalline domains of both polymers adopt a stacked-lamellar morphology, consisting of alternating crystalline lamellae and amorphous interlayers, that comprise MAF and RAF. Lateral dimensions of both the crystal lamella, including its thickness L_c, as well as the amorphous interlayer thickness L_a, are dependent on the applied crystallization conditions.[15,17]

The interest in enzymatic recyclability of semicrystalline polyesters started with the description of PET-degrading enzymes in the early 2000s. Later, research interest grew with the discovery of IsPETase.[18] This sparked searches for new enzymes as well as protein engineering efforts to improve enzyme activity and thus degradation efficiency. Currently, multiple highly efficient PET-hydrolases have been identified, which are capable of degrading at least amorphous PET up to 100% within 24 h.[5,19–27] In contrast, enzymatic hydrolysis of PBT remains largely unexplored. A few studies reporting on enzymatic PET degradation included PBT as an alternative substrate, but only miniscule amounts of product formation could be observed.[19,28,28–31]

Studies on PET have shown that increased crystallinity severely inhibits enzymatic degradation. Depending on the enzyme variant, substrate release is reduced close to zero for crystallinities exceeding 18%–25%.[32–36] This sensitive reaction of the enzyme toward crystallinity is primarily attributed to the reduced chain mobility and increased molecular packing within crystalline regions, which restricts access to the polymer chains. In addition to the reduced degradation rate, several studies have reported a noticeable delay in product release when working with highly crystalline PET substrates.[32,33] Further, the effect of MAF and RAF on the product release was investigated, whereby it was found that MAF seemed to degrade faster than RAF.[33]

Previous studies have shown that semicrystalline morphology plays a critical role in the enzymatic degradability of PET.[32–36] In contrast, studies involving PBT have thus far only relied on commercially available materials, which likely exhibit degrees of crystallinity beyond the threshold tolerated for enzymatic hydrolysis. This suggests that PBT degradation may be feasible if its semicrystalline properties are optimized, and appropriate incubation conditions are applied.

In this study, we demonstrate that PBT can be enzymatically hydrolyzed to a significant extent by tailoring enzyme and substrate conditions. An immense improvement in enzymatic PBT degradation is achieved by increasing the incubation temperature far beyond T_g. We explored different degradation conditions for PET and PBT using variants of the Leaf-Branch Compost Cutinase (LCC) enzyme[37] and observed different profiles, including temperature, enzyme concentration, and overall efficiency at the respective optimal conditions. We further identified which semicrystalline features—such as fractional composition (MAF, RAF, and crystalline fraction) and lamellar structure dimensions (L_c and L_a)—most significantly influence enzymatic degradability of PBT. Therefore, a series of substrates with systematically varied semicrystalline properties was prepared through rapid quenching followed by controlled isothermal annealing. These substrates were then subjected to enzymatic hydrolysis to assess their degradability.

2. Results and Discussion

2.1. Annealing of Quenched PBT

To assess the influence of variations in the semicrystalline morphology of PBT on enzymatic degradability, PBT substrate properties were systematically modified through isothermal annealing from the glassy state. In the following, the influence of annealing on the polymer's fractional composition is analyzed, including X_c, the total amorphous fraction (TAF), and its sub-fractions—MAF and RAF. Additionally, the impact of annealing on crystalline morphology is examined, with particular focus on the dimensions of L_c, L_a, and their sum, the long period (LP).

2.2. Influence of Isothermal Annealing on Fractional Composition

The impact of thermal treatment on fractional composition was assessed using differential scanning calorimetry (DSC) and modulated DSC (MDSC) data. **Figure 1** illustrates the variation of TAF, MAF, and RAF as a function of annealing temperature, T_{anneal}, with detailed parameter values provided in **Table 1**. In the quenched state, PBT exhibits a high proportion of MAF and RAF. Upon annealing at any T_{anneal}, MAF is gradually converted into RAF and X_c, restricting chain mobility and reducing free volume. Between the annealed samples, as T_{anneal} increases, TAF steadily decreases, while MAF and RAF exhibit a more complex trend. Above 140 °C, increased chain mobility seems to prevent RAF formation, as polymer chains preferentially align with existing crystalline surfaces instead of becoming immobilized in the rigid amorphous phase. Conversely, at temperatures below 130 °C, reduced chain mobility seems to limit crystallization, leading to an increased RAF fraction. This shift in crystallization behavior observed around 130 °C aligns well with findings reported in the literature, where a change in the isothermal crystallization process as well as a minimum in crystallization time has been identified for PBT within the 120–130 °C range.[38] The above-described

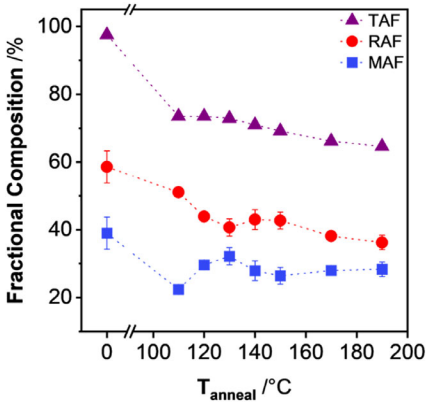

Figure 1. Total (TAF), mobile (MAF), and rigid (RAF) amorphous fractions of PBT obtained from MDSC and DSC data as a function of annealing temperature. Dotted lines are used as a guide to the eye. For all graphs, error bars correspond to the standard deviation from three independent experiments.

Table 1. Structural properties of quenched and annealed PBT substrates and their product release under enzymatic degradation at 80 °C. The substrate number corresponds to the applied annealing temperature. All standard deviations arise from three independent measurements.

Sample Number	T_{anneal} [°C]	X_c [%]	MAF [%]	RAF [%]	n	TAF [%]	LP [nm]	L_c [nm]	L_a [nm]	Total Product Release [mM]
Quench	–	2.5 ± 1.0	39.0 ± 4.7	58.5 ± 4.7	–	97.5 ± 1.0	–	–	–	1.73 ± 0.30
110	110	26.6 ± 0.2	22.4 ± 1.1	51.0 ± 1.1	1.98	73.4 ± 0.2	6.03	1.90	4.13	1.08 ± 0.11
120	120	26.5 ± 0.7	29.6 ± 1.2	43.9 ± 1.2	–	73.5 ± 0.7	6.01	1.79	4.22	0.97 ± 0.19
130	130	28.0 ± 1.2	32.2 ± 2.5	40.7 ± 2.5	1.86	72.0 ± 1.2	6.67	2.06	4.61	0.94 ± 0.45
140	140	29.0 ± 0.1	27.9 ± 2.9	43.0 ± 2.9	–	71.0 ± 0.1	6.65	1.95	4.70	0.66 ± 0.06
150	150	30.8 ± 0.8	26.4 ± 2.5	42.7 ± 2.5	1.93	69.2 ± 0.8	7.51	2.28	5.23	0.50 ± 0.05
170	170	33.9 ± 0.4	28.0 ± 0.6	38.2 ± 0.6	1.70	66.1 ± 0.4	8.88	2.69	6.20	0.17 ± 0.02
190	190	35.4 ± 0.5	28.4 ± 2.1	36.2 ± 2.1	1.83	64.6 ± 0.5	11.20	3.31	7.92	0.07 ± 0.01

variations in fractional composition allow for the evaluation of their influence on the enzymatic degradability of the PBT substrate.

2.3. Influence of Isothermal Annealing on Crystallization Kinetics and Lamellar Substructure

To obtain the impact of the annealing treatment on the resulting crystalline morphology, a combination of isothermal Avrami analysis and X-ray scattering techniques was employed. The crystallization kinetics and the dimensionality of crystal growth can be obtained from isothermal Avrami studies at different temperatures corresponding to the employed T_{anneal}. For this, quenched PBT was rapidly heated in a DSC to the respective T_{anneal}, where it underwent isothermal recrystallization. The corresponding DSC traces are provided in (Figure S1, Supporting Information). In all samples, the crystallization peak appeared at ≈15 s, indicating the inherently fast crystallization rate of PBT. From the DSC traces, the relative crystallinity over time could be calculated. That was then used to calculate the Avrami plots (**Figure 2**a). The Avrami exponent n, which describes the nucleation process, growth constraints, and dimensionality of crystal growth, was determined from the slope of the Avrami plot within the 20%–80% crystallinity range.[39] For all samples, n was found to be between 1.70 and 1.98 (Table 1). Depending on the nucleation and growth constraints, n can indicate different dimensionalities of growth. For the annealed PBT samples, likely instantaneous heterogeneous nucleation takes place at preexisting nuclei that were seemingly already present in the quenched PBT. Thus, no prolonged nucleation phase takes place during annealing. In this case, $n \approx 2$ suggests a 2D, platelet-like lamellar growth mechanism, with the absence of any larger three-dimensional spherulitic structures.[39] Consequently, in the following, only the impact of lamellar dimensions on the enzymatic degradation needs to be investigated, as any overlaying effects from spherulitic superstructures can be ruled out.

To further analyze the lamellar structure, verified by Avrami analysis, small-angle X-ray scattering (SAXS) and wide-angle X-ray scattering (WAXS) were employed. WAXS data (Figure S2b, Supporting Information) reveal that the quenched sample exhibits no sharp Bragg peaks corresponding to crystalline structures. This indicates an extremely low crystallinity and a lack of ordered crystalline regions for quenched PBT. In contrast, all annealed samples display Bragg peaks. With increased T_{anneal}, the Bragg Peaks increase in their intensity and decrease in their full-width-at-half-maximum, signifying an increase in crystallinity and an increase in the lamella size in all spatial directions.[40] Based on the Bragg peak positions (8.9°, 15.9°, 17.1°, 20.4°, 23.1°, 25.0°), it can be confirmed that all annealed samples adopt the α-crystal polymorph of PBT.[41] To calculate the size of the

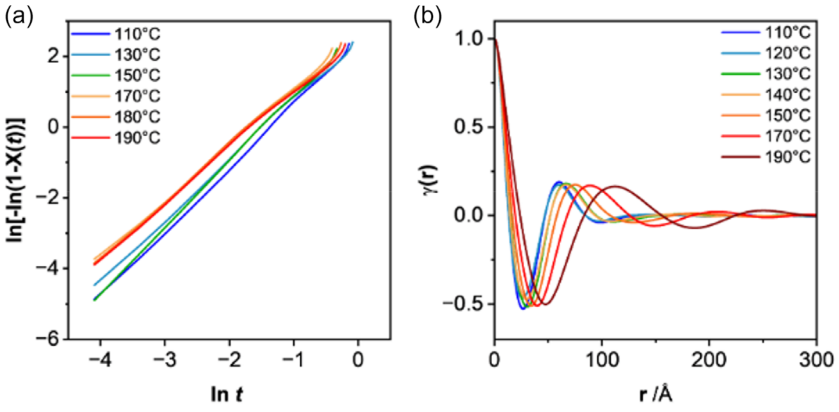

Figure 2. Crystallization kinetics and lamellar substructure of the differently annealed PBT substrates. a) Isothermal crystallization kinetics: Avrami curves of quenched PBT at different T_{anneal} obtained from isothermal DSC data. b) Lamellar substructure: 1D correlation function calculated for differently annealed PBT samples obtained from 1D SAXS diffractograms. The LP was extracted from the first maximum, while L_c was determined from the inflection point of the initial decay.

crystalline lamella in *Z*-direction, L_c, SAXS data using 1D correlation function analysis was employed (Figure 2a). The quenched sample exhibited no scattering maxima in SAXS data (Figure S2a, Supporting Information). Consequently, correlation analysis was not applied to this sample. In contrast, all annealed samples displayed visible SAXS intensity maxima, highlighting the presence of ordered crystalline structures and thus validating the correlation function analysis (Figure 2a). The LP was extracted from the first maximum of the correlation function $\gamma(r)$, while L_c was determined from the inflection point of the initial decay in $\gamma(r)$, following the method of Strobl and Schneider.[42] The analysis shows that all lamellar substructures increase in thickness with rising T_{anneal} (Table 1). At higher T_{anneal}, improved chain mobility facilitates crystal growth, resulting in thicker crystalline lamellae, whereas lower T_{anneal} restricts mobility, limiting structural development.[17] Particularly noteworthy is the increase in the amorphous interlayer thickness L_a, as it may be relevant for enzymatic degradation. LCC has a diameter of about 45 Å (pdb id: 4eb0). If L_a exceeds the enzyme´s diameter, enzymatic degradation might be enhanced, as the comparably smaller enzyme might be able to penetrate crystalline stacks by progressing along the amorphous interlayers between individual crystal lamellae. If this hypothesis is held, an L_a larger than the enzyme´s diameter should correspond to improved degradation efficiency, marking the importance of the dimensions of semicrystalline structures.

In conclusion, annealing-quenched PBT at different T_{anneal} allows precise control over its fractional composition and the dimensions of its lamellar substructures, as demonstrated by thermal and structural analyses. The transformation of MAF into RAF and X_c with increasing T_{anneal} influences chain mobility, crystallinity, and overall morphology. Additionally, higher T_{anneal} promotes the growth of thicker crystalline lamellae and amorphous interlayers, which may impact enzymatic degradation. The achieved variations in crystalline and amorphous fractions and domain sizes provide a well-defined framework to systematically study the relationship between semicrystalline morphology and enzymatic degradation efficiency of PBT.

2.4. Enzyme Selection and Identification of Optimal Incubation Conditions for PBT Degradation

The choice of enzyme is a prerequisite for successful and efficient depolymerization. To find the ideal candidate for PBT, known PET-hydrolases, including IsPETase[18] and variants of LCC[37] and PET6,[43] were screened for their capability to degrade PBT at different temperatures (Figure S6, Supporting Information). For the LCC-derived variants, the highest soluble monomer release was detected, and activity profiles using varying enzyme concentrations were recorded utilizing PET and PBT-coated 96-well plates, respectively. These included LCC_{iccg} and LCC_{wccg}, as well as a newly generated LCC_{lccg} variant. We introduced leucin at position 243 in LCC_{lccg}, as this residue is found in the active site of PHL7 and is known to contribute to its activity.[27]

The release of soluble monomers was monitored after 24 h at various temperatures for 200 and 1000 nM enzyme concentration (**Figure 3**a, S4, Supporting Information). Temperature dependance is equal for all variants on PET, with the optimum reached at 70 °C, which is consistent with the original study describing LCC variants.[37] Similar to previous studies on enzymatic PBT degradation, only very low activity was detected between 40–50 °C, which corresponds to the T_g of PBT.[16,28–30] At 60 °C, soluble product release starts to increase, with a strong boost observed at 80 °C (Figure 3a, S4, Supporting Information). At the two enzyme concentrations, differences between the variants become apparent. At a concentration of 200 nM, LCC_{iccg} degrades PBT best, followed by LCC_{lccg} and LCC_{wccg}, with an almost twofold difference. The trend is even more prominent at a concentration of 1000 nM, with LCC_{iccg} increasing soluble product release up to 1.5 mM, followed closely by LCC_{lccg}, while LCC_{wccg} shows reduced degradation (Figure S4, Supporting Information).

To understand these opposing behaviors, the influence of enzyme concentration was studied for both polyesters at 60 and 80 °C. (Figure 3b, S5, Supporting Information). While on PET, both variants show very similar degradation profiles; significant differences could be observed when targeting PBT. LCC_{iccg}

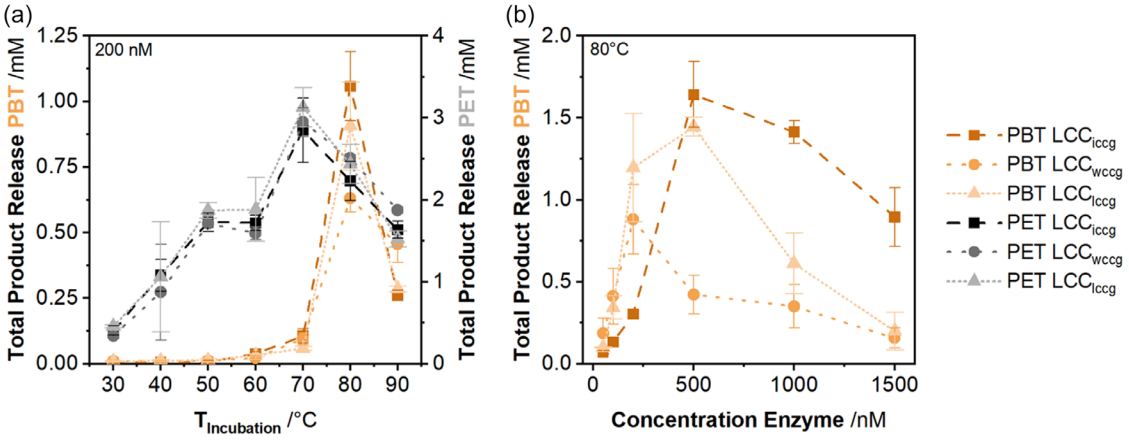

Figure 3. Degradation profiles of LCC-variants: a) total product release at various $T_{incubation}$ for PBT and PET treated with 200 nM enzyme (LCC_{iccg}, LCC_{lccg}, or LCC_{wccg}) solution for 24 h. ($n = 3$). b) Total product release for PBT treated with various enzyme concentrations of LCC_{iccg}, LCC_{lccg}, or LCC_{wccg} for 24 h at 80 °C ($n = 4$). Dotted lines are used as guide to the eye.

turns out to be the superior candidate in terms of total product release and resistance toward concentration-dependent self-inhibition (Figure 3b). Although a decrease in soluble product release can be observed above 1000 nM for LCC_{iccg}, this effect occurs much earlier in LCC_{wccg}, showing optimal degradation at 200 nM enzyme concentration. Variant LCC_{lccg} has an intermediate profile with an optimum at 500 nM, but similar inhibition at higher concentrations as LCC_{wccg}. While previously described for mesostable PET-hydrolases on PET,[44] this inhibitory effect for highly thermostable LCC variants could only be observed on PBT and is more pronounced at higher temperatures (Figure 3b, S5, Supporting Information). Avilan et al.[44] proposed flexibility around the active site to be a main contributor toward concentration-dependent inhibition. They were able to reduce this inhibitory effect in *Is*PETase by introducing stabilizing mutations. The necessary increase in incubation temperature might force more flexibility around this region in the otherwise very stable LCC-variants. The combination of this additional flexibility with the different availability of suitable attack sites, when comparing PET and PBT, might lead to this differing degradation behavior. The reduced activity of LCC_{wccg} on PBT is likely caused by the bulkiness of Trp at position 243, which is in structural proximity to the active site, restricting favorable interactions of the enzyme with multiple polymer subunits, thereby impeding efficient hydrolysis (Figure S7, Supporting Information).

Concluding these experiments, incubation of PBT at 80 °C with 500 nM of LCC-iccg was determined as an ideal setup for enzymatic PBT depolymerization and has been used in subsequent experiments. This high $T_{incubation}$ required for PBT was surprising, as PET depolymerization suggests that optimal degradation happens around T_g, and higher temperatures are shown to decrease degradability, likely due to recrystallization.[36,37] Since the inherent activity profile of LCC_{iccg} and the T_g of the substrate cannot account for the shift of $T_{incubation}$ to higher temperatures, other material properties of PBT must be responsible. Therefore, we examined the influence of PBT's semi-crystalline properties on its degradability, aiming to explain this phenomenon.

2.5. Influence of Degree of Crystallinity on Enzymatic Degradation with LCC_{iccg}

The effect of fractional composition and crystalline substructures on the enzymatic degradability of PBT was assessed by monitoring the release of soluble degradation products during incubation at 80 °C, using ultra-high-performance liquid chromatography (UHPLC). When correlating total product release as a function of crystallinity for enzyme-treated samples (**Figure 4**a), a linear correlation is observed between 25% and 40%. Control samples exhibited negligible product release

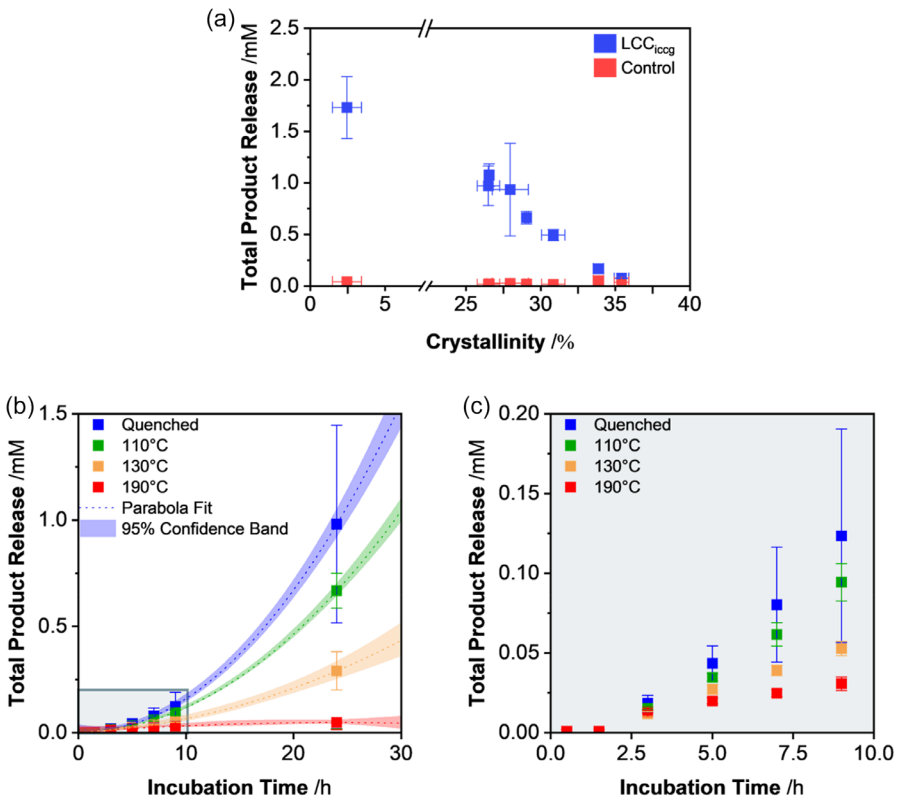

Figure 4. a) Product release after 24 h and b,c) time-dependent total product release of PBT substrates with different crystalline properties: (a) total product release as a function of crystallinity after 24 h at 80 °C for samples treated with 500 nM LCC_{iccg} (blue) and with borate buffer as control (red), (b) time-dependent total product release of samples treated with 500 nM LCC_{iccg} at 80 °C with a parabolic fit (dotted line) and associated 95% confidence interval (shaded area), (c) magnified view of the initial hours of time-dependent product release from (c). For all graphs, error bars correspond to the standard deviation from three independent experiments.

(Table S1, Supporting Information), confirming that autohydrolysis does not significantly contribute to the degradation of PBT.

In the case of the quenched PBT sample, which had the lowest degree of crystallinity, 1.73 mM of soluble products were released after 24 h of incubation (Table 1). This highlights that PBT is enzymatically degradable when its material properties are appropriately modified. However, as crystallinity increases, total product release declines progressively. Once crystallinity surpasses 32%, degradation becomes negligible. For PBT grades processed using conventional methods such as injection molding and conventional extrusion, crystallinities typically are above 40%.[16] Thus, the crystallinity levels in commercially available PBT products make them either minimally or not enzymatically degradable. For PET, this correlation between total product release and crystallinity has also been found.[32,34,35] These studies have attributed this sensitivity of enzymes to changes in crystallinity to the dense chain packing and high rigidity of crystalline and RAF regions. Specifically, enzymatic degradation of polyesters is proposed to occur in two stages. Initially, the enzyme randomly binds to a segment of the polymer chain and performs an endo-type cut, generating two new chain ends without immediately releasing soluble degradation products. In the second step, if the polymer chains exhibit sufficient mobility and low packing density, the enzyme moves along the chain, cleaving adjacent ester bonds in an exo-type manner, thereby releasing soluble degradation products. However, in highly crystalline or RAF-rich regions, enzyme movement along the chain is restricted, likely resulting in a time-consuming desorption-rebinding process at a new, distant site. Consequently, exo-type cuts are limited, reducing the overall release of degradation products.[35]

Re-crystallization of the PBT samples due to the elevated incubation temperature of 80 °C was also considered. However, for all annealed samples, the annealing temperatures (>110 °C) were substantially higher than the subsequent incubation temperature, making further recrystallization during the incubation unlikely. In contrast, quenched PBT samples exhibited gradual recrystallization under incubation conditions. Pretrials have shown that exposing quenched PBT to an 80 °C buffer solution for 24 h increased its crystallinity to ≈22%, which remains lower than that of the annealed samples. This gradual increase likely explains why the quenched sample deviates from the linear relationship between product release and crystallinity observed in the other samples (Figure 4a). With prolonged incubation, further recrystallization is observed, with crystallinity reaching around 29% after 120 h. Due to this recrystallization effect, the degradation efficiency of quenched PBT might in fact be higher.

The difference in the degradability of the samples with different fractional compositions can further be observed in scanning electron microscopy (SEM) images. For the control sample (Figure S3, Supporting Information), the surface remains smooth after incubation, showcasing that the incubation at 80 °C in buffer solution has no degrading effect, as already suggested by UHPLC (Figure 4a). However, for all enzyme-treated samples, surface alterations are visible (**Figure 5**). These become more pronounced with decreasing substrate crystallinity and thus increasing TAF. For the quenched sample (Figure 5a), porous structures are visible on the entire surface. Similar degradation patterns were found for PET, whereby the depth and width of the pores were proposed to depend on the employed enzyme variant.[24,34,35,45]

For samples annealed at 150 °C (Figure 5b) and 190 °C (Figure 5c), the surface alterations are less pronounced. For 150 °C, the entire surface shows traces of degradation, whereby the pore size in comparison to the quenched sample is significantly reduced. Remaining structures on the surface have a nodule-like shape. For 190 °C, the surface is only spot-wise degraded. Within the degraded spots, a rough structure is present.

To further investigate degradation kinetics across different crystallinity levels, time-dependent degradation studies were conducted on four selected samples (Figure 4b,c). The product release at different time stamps is listed in Table S2, Supporting Information. For all samples, the increase in product release over 24 h followed a parabolic trend, with corrected R^2 values of at least 99.5. Reaction rates determined from the parabolic fit for

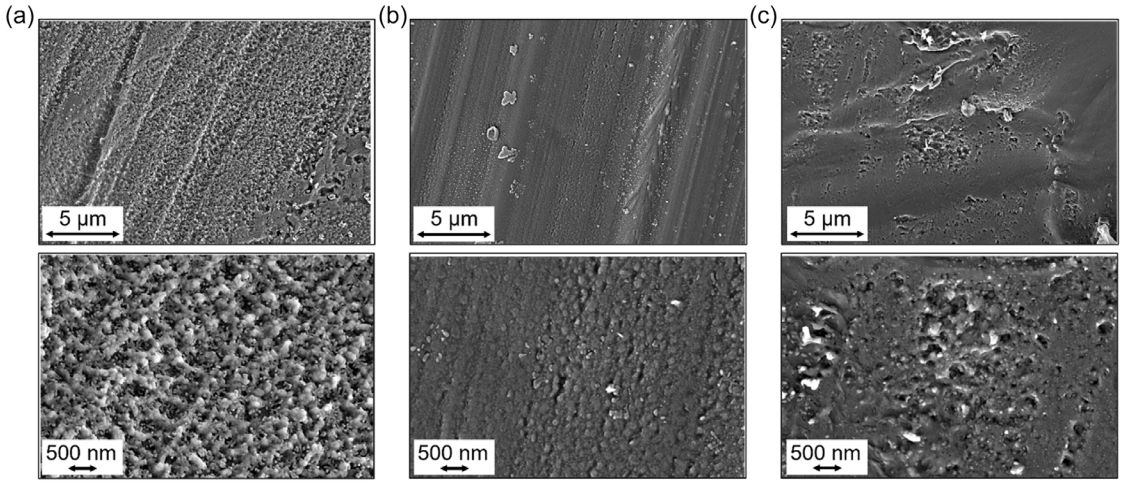

Figure 5. SEM images of a) quenched and annealed at b) 150 °C and at c) 190 °C PBT substrates after incubation in 500 nM LCC_{iccg} solution for 24 h at 80 °C.

a reaction time of 24 h are reported in Table 1. The parabolic nature of the release suggests that, for longer incubation times, even greater differences in enzymatic degradability between samples of varying crystallinity can be expected.

Interestingly, a comparison of the initial product release phase for the time-dependent samples (Figure 4c) reveals that measurable degradation begins after three hours for all samples, irrespective of their crystallinity. This lag phase has been previously observed for various PET-hydrolases. However, while some studies[32,33,46] on PET have reported prolonged lag phases for samples with higher crystallinity, this effect is not observed for PBT.

2.6. Influence of Fractional Composition on Enzymatic Degradation with LCC_{iccg}

Besides the influence of the crystalline fraction, the influence of the amorphous phase composition might exhibit an effect on the degradability of the substrate.

A clear correlation between the product release and the TAF ($100–X_c$) (**Figure 6**a) is observed. In contrast, no clear trend is apparent when considering MAF and RAF individually. Instead, total product release appears to be independent of the relative fractions of MAF and RAF within the amorphous phase. This independence is particularly evident when comparing samples annealed at 110–130 °C, which exhibit similar crystallinities but differ by more than 10% in their MAF and RAF contents (Table 1), yet all demonstrate an approximate product release of 1 mM. The opposite pattern is observed for samples annealed at 140 and 150 °C: despite nearly identical MAF and RAF contents (Table 1), the sample with a slightly higher TAF exhibits higher product release. These findings suggest that, for PBT, the enzyme might not differentiate between MAF and RAF, nor is MAF preferentially or more rapidly degraded. In contrast, studies on PET have shown a strong correlation between MAF content and product release, suggesting that MAF in PET is preferentially degraded and likely exhibits a higher degradation rate than RAF.[33] The different degradation behaviors of PBT and PET can be explained by the interplay of their devitrification temperatures, phase compositions, and the plasticizing effect of water during incubation. In PBT, the T_g of MAF ($T_{g,MAF}$) ranges between 40 and 50 °C, whereas $T_{g,RAF}$ is reported to be ≈101 °C.[12,13] RAF also represents a substantial portion of the polymer (36%–51%), whereas MAF typically makes up only 22%–32% (Table 1). In contrast, PET exhibits a $T_{g,MAF}$ of around 75 °C and a proposed $T_{g,RAF}$ of ≈200 °C, with RAF typically constituting only 3.6%–20%, depending on thermal history.[14]

Water uptake during incubation further reduces the effective T_g of both polyesters, since water acts as a plasticizer by decreasing intermolecular interactions. For PET, a 15 °C depression of $T_{g,MAF}$ was observed under 100% humidity.[47–49] While RAF likely absorbs slightly less water due to its denser packing, a similar effect can be expected. Taking this into account, the effective glass transition temperatures can be estimated to be lowered to ≈60 °C (MAF) and 190 °C (RAF) for PET, and 35 °C (MAF) and 90 °C (RAF) for PBT. Moreover, devitrification does not occur at a single, sharp temperature but typically proceeds over a range of 5–20 °C around the nominal T_g.[50]

These differences have direct implications for their enzymatic degradation. In PET, the extremely high $T_{g,RAF}$ means that under typical incubation conditions (60 °C), only MAF is mobile, leading to a preferential degradation of MAF over RAF, as found in previous studies.[33] However, because RAF represents only a minor fraction of PET and enzyme activity is already optimized for this polymer, sufficient degradation still occurs. In PBT, by contrast, both $T_{g,MAF}$ and $T_{g,RAF}$ are below or close to the optimal incubation temperature of 80 °C. As a result, both fractions become mobile during incubation, explaining their comparable degradation rates. The predominance of RAF in PBT further explains why substantial product release is only observed when incubation temperatures approach the RAF devitrification region (around 90 °C). However, because LCC variants begin to denature above 90 °C, product release declines again at higher temperatures (Figure 3).

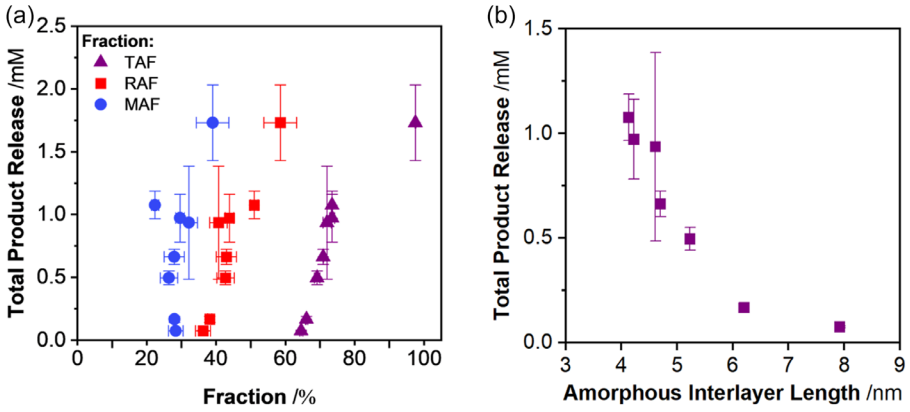

Figure 6. Comparison between a) impact of fractional composition and b) dimensions of amorphous interlayer on total product release shows TAF is the predominant influencing factor on degradability. (a) Total product release (500 nM LCC_{iccg} solution, 24 h, 80 °C), dependent on the fractional composition, including MAF, RAF, and TAF, of the samples, (b) total product release (500 nM LCC_{iccg} solution, 24 h, 80 °C), dependent on amorphous interlayer length L_a of the samples. For all graphs, error bars correspond to the standard deviation from three independent experiments.

2.7. Influence of the Dimensions of Lamellar Substructures on Enzymatic Degradation with LCC_{iccg}

As discussed earlier, the fractional composition and thermal characteristics significantly influence substrate degradability. However, the effect of the dimensions of the lamellar substructures must be additionally evaluated. As previously suggested, a L_a exceeding the enzyme's diameter might facilitate degradation, since the comparably smaller enzyme might penetrate into crystalline stacks more easily by progressing along the amorphous interlayers that are located between the individual crystal lamellas. However, samples with the largest L_a (Figure 6b) exhibit the lowest product release. Similarly, for LP and L_c, an exponential decline in product release is observed as their thicknesses increase (Table 1). This decline, however, originates from the exponential relationship between X_c and the lamellar properties (Table 1) rather than any direct adverse effect of increasing LP, L_c, or L_a on substrate degradability. Therefore, the length scales of the lamellar substructure do not have a significant impact on product release at the currently achievable degradation stages. This may be because, in the case of nonspherulitic materials during the early stages of degradation, sufficient material outside lamellar stacks is available, reducing the need for the enzyme to penetrate the amorphous interlayers within the stacks to achieve product release.

This suggests that, at least under the currently achievable degradation stages and for nonspherulitic substrates, the overall amount of degradable material, which is the TAF in the case of PBT, is significantly more important than the dimensions of the amorphous lamellar interlayers.

3. Conclusion

Enzymatic degradation of PBT was significantly improved by systematically optimizing reaction conditions. The enzyme LCC_{iccg} was identified as the most efficient catalyst for PBT degradation, with elevated temperature being an important factor. This effect can be understood when analyzing the properties of the semicrystalline substrate, including the fractional composition of mobile, rigid, and total amorphous fractions (MAF, RAF, TAF), as well as the dimensions of lamellar substructures such as the amorphous interlayer thickness. Additionally, incubation conditions, specifically enzyme concentration and incubation temperature, were optimized. Significant enzymatic degradation of PBT could be achieved by tuning both the substrate's semicrystalline properties and the reaction conditions.

Analyses showed that polymers with a high content of RAF require incubation temperatures within the effective RAF devitrification range to achieve sufficient chain mobility across large parts of the substrate, consequently enabling significant enzymatic degradation. At 80 °C, both MAF and RAF in PBT exhibit increased mobility, resulting in significant degradation for both fractions with comparable rates. For successfully quenched PBT ($X_c = 2.5 \pm 1\%$), incubation at 80 °C with 500 nM LCC_{iccg} achieved a product release of 1.7 mM within 24 h. Reducing nondegradable crystalline domains through quenching was essential for this enhanced degradation.

The results demonstrated that the quantity of the degradable fraction, which is the total amorphous content for PBT, is the decisive factor governing degradability. In contrast, the dimensions of the crystalline and amorphous domains showed no measurable influence on enzymatic hydrolysis within the observed time frame. Importantly, there is also an effect on protein flexibility induced by the increase in temperature, which supports formation of interactions with the material surface. This is in accordance with the observed concentration-dependent inhibition of PBT degradation through the LCC variants, as this effect has been attributed to active site flexibility for some PET-degrading enzymes as well.[44]

Overall, these findings highlight the importance of understanding the fractional composition and thermal characteristics of semicrystalline substrates for enabling enzymatic degradation of polymers previously regarded as recalcitrant. Moreover, the results indicate that targeted preprocessing strategies, such as crystallinity reduction, are key to facilitating efficient enzymatic hydrolysis of PBT. A deeper understanding of the interplay between polymer structure and enzyme characteristics is crucial for advancing and optimizing enzymatically driven recycling processes for polymeric materials.

4. Experimental Section

Materials

Commercially available PBT and PET materials were used. PBT B 6550 was provided by BASF SE (Ludwigshafen am Rhein, Germany). CleanPET was provided by Veolia Umweltservice GmbH (Bayreuth, Germany).

Protein Production and Purification

Plasmids for expression of the LCC variants were generated via site-directed mutagenesis using pET21-LCC_{wccg} as template. T7 Shuffle cells were transformed with a pET21 vector harboring the enzyme's gene sequence. Terrific Broth (TB) medium was inoculated and grown at 30 °C up to an optical density at 600 nm of 1.0. Expression was induced by adding 300 mM isopropyl-β-D-thiogalactopyranoside (IPTG), and cells were grown overnight at 16 °C. After harvesting via centrifugation at 3990 × G for 15 min, the pellets were resuspended in binding buffer (300 mM NaCl, 50 mM phosphate, 50 mM imidazole, pH 7.4). Cells were lysed via sonification, and insoluble substances were removed via centrifugation at 39,190 × G for 1 h. A Ni-IMAC was performed with a linear gradient from binding buffer to 100% elution buffer (300 mM NaCl, 50 mM phosphate, 400 mM imidazole, pH 7.4). The pooled fractions were dialyzed overnight against 50 mM phosphate, pH 7.4, at 4 °C. Aggregates that formed during concentration were removed via filtration with a 0.22 μm filter. An additional dialysis into storage buffer (25 mM HEPES, 150 mM NaCl, pH 7.4) has been performed at 4 °C overnight. After further concentration and filtration, aliquots were flash-frozen with liquid nitrogen and stored at −80 °C.

Preparation of PBT Substrates

For optimizing incubation conditions (see above), 96-well microtiter plates were coated with PET or PBT according to Weigert et al.[51] with the exception that for PBT, the drying time was reduced to 10 min. Dripping times were 90 s for PET and 30 s for PBT. Quenched PBT was produced by efficiently quenching an extruded polymer melt in a quench bath, whereby filaments with a diameter of 0.6 mm were obtained. Isothermal annealing of the quenched PBT was conducted in a heated silicon oil bath for 1 min at temperatures between 110 and 190 °C. After annealing, the annealed samples were directly transferred to a quenching bath to prevent further crystallization.

Hydrolysis of PBT Substrates

For the temperature and concentration sweep trials of PET and PBT, the substrate-coated 96-well plates were incubated with 50 μL of enzyme solution consisting of an assay buffer (50 mM NaCl, 50 mM Borate, pH 8.5) for 24 h in a water bath at the respective temperature. To prevent evaporation of the solution, the well plate was covered with gas-tight adhesive film. The influence of temperature was tested with 200 and 1000 nM enzyme, while the concentration dependency was investigated at 60 and 80 °C. Individual plates were prepared for each combination of polymer and temperature. For all non-time-dependent incubations of PBT filaments, 4 × 5 mm long cuttings were placed in an untreated 96-well microtiterplate. 150 μL of enzyme solution consisting of an assay buffer (50 mM NaCl, 50 mM Borate, pH 8.5) and 500 nM LCC-iccg was added to the samples. Incubation was carried out at 80 °C for 24 h. To prevent evaporation of the solution, the well plate was covered with gas-tight adhesive film. For the time-dependent incubation of PBT filaments, the reaction volume had to be increased. However, the ratio between substrate surface to enzyme solution volume was kept constant. Thus, for the time-dependent experiment, 27 × 5 mm long PBT filament cuttings were placed in Eppendorf tubes with 1 mL of enzyme solution consisting of 500 nM enzyme and an assay buffer (50 mM NaCl, 50 mM Borate, pH 8.5). At multiple time steps (0.5, 1.5, 3, 5, 7, 9, 24 h), 50 μL of the reaction solution was taken for UHPLC analysis and frozen immediately. To prevent a reduction of the solution:substrate ratio, 50 μL of enzyme solution was added subsequently, whereby this solution was kept at 80 °C for the same time as the degradation samples. Dilution of the samples throughout the experiment has been taken into account in the calculation of total product release. All enzyme-treated and control samples were incubated and measured at least in triplicate.

Thermal Analysis

The degree of crystallinity X_c and isothermal crystallization kinetics were determined by Differential Scanning Calorimetry (DSC) on a DSC 1 from Mettler Toledo (Columbus, OH, USA). To obtain X_c, the samples were heated from 0 to 250 °C with a heating rate of 10 K min^{-1} and a nitrogen flow of 50 mL min^{-1}. The heat of fusion of 100% crystalline PBT was assumed to be 140 J g^{-1}.[52] The analysis was performed threefold.

For the isothermal crystallization studies, quenched PBT was heated up from 25 °C to the desired T_{anneal} (110, 120, 130, 150, 170, 180, 190 °C) with a heating rate of 300 K min^{-1}.T_{anneal} was maintained for 10 min to allow for complete crystallization. The nitrogen flow was 50 mL min^{-1}. Following the Avrami theory,[53,54] crystallization kinetics were determined from the isothermal DSC data. The Avrami exponent n was evaluated from the slope of the Avrami plot between 20% and 80% crystallinity.

The content of mobile amorphous fraction (MAF) was determined with modulated DSC (MDSC) on a Q1000 from TA Instruments (New Castle, DE, USA). The samples were heated from −50 to 250 °C with a heating rate of 2 K min^{-1}, a period of 40 s, and a modulation amplitude of 0.212. The nitrogen flow was 50 mL min^{-1}. MAF was determined from the change in heat capacity ΔCp at the glass transition temperature following Equation (1).

$$\mathrm{MAF} = \frac{\Delta C_p}{C_{p,\mathrm{amorphous}}} * 100 \quad (1)$$

Where ΔC_p is the change in heat capacity of the sample and $\Delta C_{p,amorphous}$ is the change in heat capacity for 100% amorphous PBT, which is equal to 0.35 J g^{-1} K^{-1}.[13] RAF was then calculated using Equation (2).

$$\mathrm{RAF} = 100 - X_c - \mathrm{MAF} \quad (2)$$

X-Ray Analysis

Structural properties of the samples were analyzed by small- and wide-angle X-ray scattering measurements, which were performed using a Xeuss 3.0 from Xenocs (Grenoble, France) equipped with a copper source ($\lambda = 1.5418$ Å) and an Eiger2 R 1 M detector from Dectris (Baden, Switzerland). The detector had 1028 × 1062 pixels and a pixel size of 75 μm × 75 μm and was located 0.0514 m from the sample for WAXS, 0.601 m for intermediate q-regions, and 1.80 m for SAXS. The beam size was adjusted to 0.5 × 0.5 mm. Each sample was measured for 1 h at each sample-detector distance in vacuum. The measured single SAXS and WAXS images were radially averaged, and the respective 1D diffractograms were extracted. The 1D diffractograms were merged with overlap regions of 0.03–0.1 Å^{-1} and 0.07–0.1 Å^{-1} within XSACT 2.6 (Xenocs). The lamellar parameters long period (LP), crystal layer thickness (L_c), and amorphous interlayer thickness (L_a) were determined by 1D correlation function analysis using SASView 6.0.1. The experimental data were extrapolated with Guinier and Porod fits for low and high q-regions, respectively. To calculate the Guinier Fit, scattering data between 0.01 and 0.013 Å^{-1} was used. For the Porod Fit, the starting data point was set to after the peak of the scattering data, which was between 0.14 and 0.2 Å^{-1}. The end point for the Porod Fit was 0.4 Å^{-1} for all samples. LP was extracted from the first maximum of the obtained 1D correlation function $\gamma(r)$, while L_c was determined from the inflection point of the initial decay in $\gamma(r)$, following the method of Strobl and Schneider.[42] L_a was automatically determined via the program by employing Equation (3).

$$L_a = \mathrm{LP} - L_c \quad (3)$$

Surface Analysis

The surface morphology of the degraded samples was evaluated by SEM on a Zeiss Ultra Plus from Carl Zeiss AG (Oberkochen, Germany) that was equipped with a tungsten cathode and an SE2 detector. The samples were sputtered with 2 nm of platinum using a Platinum-Sputter Coater 208HR from Cressington Scientific Instruments (Watford, UK). Subsequently, the samples were sputtered with 20 nm of carbon using an EM ACE 600 Sputter Coater from Leica Microsystems (Wetzlar, Germany).

Analysis of Soluble Degradation Products

To monitor the water-soluble degradation products, all incubated samples were analyzed by ultra-high-performance chromatography (UHPLC) using a Thermofisher RS3000 UHPLC system equipped with a Phenomenx Kinetix 1.7 μm EVO C18 (50 × 2.1 mm, 100 Å) reversed-phase column. For sample preparation, 50 μL of the incubation solution was mixed with four parts of acetonitrile containing 1% formic acid. The solution was centrifuged at 4500 × g for 10 min. 1 μL of the supernatant was introduced into the column, which was heated to 55 °C. In the column gradient from 100% solvent 1 (H_2O + 0.1% trifluoroacetic acid) to 80% solvent 2 (acetonitrile) and 20% solvent 1 was applied at a flow rate of 1.3 mL min^{-1}. The amounts of soluble degradation products (TA, MHET, and BHET for PET; TA and MHBT for PBT) were quantified based on calibration runs.

Acknowledgements

The authors are very grateful to BASF SE (Ludwigshafen am Rhein, Germany) for generous funding and for providing different Ultradur (Polybutylene terephthalate) grades. The authors thank J. Sloan, T. L. Ellinghaus, and G. Krauss for project supervision and guidance, and critical feedback on the manuscript. The authors acknowledge Lara Schatt for support with enzyme preparation and measurements, Christopher Greve and the Herzig Group at the University of Bayreuth for carrying out the X-ray measurements, and the DFG for provision of INST 91/443-1, as well as Annika Pfaffenberger and the Bavarian Polymer Institute (BPI) for taking and providing access to SEM measurements. Further, this work benefited from the use of the PET degradation platform, originally developed under DFG project no. 391977956 (SFB 1357, project C03), as well as the use of the SasView application, originally developed under NSF Award DMR-0520547. SasView also contains code developed with funding from the EU Horizon 2020 program under the SINE2020 project grant no. 654000.

Open Access funding enabled and organized by Projekt DEAL.

Conflict of Interest

The authors declare no conflict of interest.

Author Contributions

Annalena Pongratz: conceptualization (equal); data curation (equal); formal analysis (equal); investigation (equal); methodology (equal); project administration (equal); visualization (lead); writing—original draft (lead); writing—review & editing (equal), **Andreas Gagsteiger**: conceptualization (equal); data curation (equal); formal analysis (equal); investigation (equal); methodology (equal); visualization (supporting); writing original draft (supporting); writing—review & editing (equal), **Birte Höcker**: conceptualization (equal); funding acquisition (equal); supervision (equal); validation (equal); writing—original draft (supporting); writing—review & editing (equal), **Holger Ruckdäschel**: conceptualization (equal); funding acquisition (equal); supervision (equal); validation (equal); writing—original draft (supporting); writing review & editing (equal), **Annalena Pongratz** and **Andreas Gagsteiger** contributed equally to this work.

Data Availability Statement

The data that support the findings of this study are available from the corresponding author upon reasonable request.

Keywords: crystallinity · enzymatic degradation · isothermal crystallization · polybutylene terephthalate · polyethylene terephthalate-hydrolase

[1] PlasticsEurope. Annual production of plastics worldwide from 1950 to 2022. https://www.statista.com/statistics/282732/global-production-of-plastics-since-1950/.
[2] Open Access Government. The plastic timeline: How did we get here? https://www.openaccessgovernment.org/the-plastic-timeline-how-did-we-get-here/102481/.
[3] European Commission. End-of-life vehicles Regulation. https://environment.ec.europa.eu/topics/waste-and-recycling/end-life-vehicles/end-life-vehicles-regulation_en.
[4] European Commission. Plastics strategy. https://environment.ec.europa.eu/strategy/plastics-strategy_en.
[5] V. Tournier, S. Duquesne, F. Guillamot, H. Cramail, D. Taton, A. Marty, I. André, Enzymes' Power for Plastics Degradation. *Chem. Rev.* **2023**, *123*, 5612.
[6] F. Kawai, T. Kawabata, M. Oda, Current Knowledge on Enzymatic PET Degradation and Its Possible Application to Waste Stream Management and Other Fields. *Appl. Microbiol. Biotechnol.* **2019**, *103*, 4253.
[7] N. Malik, J. Li, A. Agarwal, Y. Kratish, T. J. Marks, Thermodynamically Leveraged Solventless Aerobic Deconstruction of Polyethylene-Terephthalate Plastics over a Single-Site Molybdenum-Dioxo Catalyst. *Green Chem.* **2025**, *27*, 2427.
[8] S. A. Vyavahare, B. M. Kharat, A. P. More, Polybutylene Terephthalate (PBT) Blends and Composites: A Review. *Vietnam J. Chem.* **2024**, *62*, 579.
[9] P. Gupta, B. Toksha, B. Patel, Y. Rushiya, P. Das, M. Rahaman, Recent Developments and Research Avenues for Polymers in Electric Vehicles. *Chem. Rec.* **2022**, *22*, e202200186.
[10] D. Heidrich, M. Gehde, The 3-Phase Structure of Polyesters (PBT, PET) after Isothermal and Non-Isothermal Crystallization. *Polymers* **2022**, *14*, 793.
[11] J. Menczel, B. Wunderlich, Heat Capacity Hysteresis of Semicrystalline Macromolecular Glasses. *J. Polym. Sci. Polym. Lett. Ed.* **1981**, *19*, 261.
[12] M. Pyda, E. Nowak-Pyda, J. Heeg, H. Huth, A. A. Minakov, M. L. Di Lorenzo, C. Schick, B. Wunderlich, Melting and Crystallization of Poly(Butylene Terephthalate) by Temperature-modulated and Superfast Calorimetry. *J. Polym. Sci. Part B Polym. Phys.* **2006**, *44*, 1364.
[13] B. Wunderlich, *Thermal Analysis of Polymeric Materials*, Springer, Berlin **2005**.
[14] H. Chen, P. Cebe, Vitrification and Devitrification of Rigid Amorphous Fraction of PET during Quasi-Isothermal Cooling and Heating. *Macromolecules* **2009**, *42*, 288.
[15] Y. Furushima, C. Schick, A. Toda, Crystallization, Recrystallization, and Melting of Polymer Crystals on Heating and Cooling Examined with Fast Scanning Calorimetry. *Polym. Cryst.* **2018**, *1*, e10005.
[16] G. W. Ehrenstein, *Polymer Werkstoffe*, Carl Hanser Verlag GmbH & Co. KG: München **2011**.
[17] E. W. Fischer, Effect of Annealing and Temperature on the Morphological Structure of Polymers. *Pure Appl. Chem.* **1972**, *31*, 113.
[18] S. Yoshida, K. Hiraga, T. Takehana, I. Taniguchi, H. Yamaji, Y. Maeda, K. Toyohara, K. Miyamoto, Y. Kimura, K. Oda, A Bacterium That Degrades and Assimilates Poly(Ethylene Terephthalate). *Science* **2016**, *351*, 1196.

[19] Y. Cui, Y. Chen, X. Liu, S. Dong, Y. Tian, Y. Qiao, R. Mitra, J. Han, C. Li, X. Han, W. Liu, Q. Chen, W. Du, S. Tang, H. Xiang, H. Liu, B. Wu, Computational Redesign of a PETase for Plastic Biodegradation by the GRAPE Strategy. *PNAS* **2021**, *118*.
[20] M. Furukawa, N. Kawakami, A. Tomizawa, K. Miyamoto, Efficient Degradation of Poly(Ethylene Terephthalate) with Thermobifida Fusca Cutinase Exhibiting Improved Catalytic Activity Generated Using Mutagenesis and Additive-Based Approaches. *Sci. Rep.* **2019**, *9*, 16038.
[21] F. Kawai, Y. Furushima, N. Mochizuki, N. Muraki, M. Yamashita, A. Iida, R. Mamoto, T. Tosha, R. Iizuka, S. Kitajima, Efficient Depolymerization of Polyethylene Terephthalate (PET) and Polyethylene Furanoate by Engineered PET Hydrolase Cut190. *AMB Express* **2022**, *12*, 134.
[22] H. Lu, D. J. Diaz, N. J. Czarnecki, C. Zhu, W. Kim, R. Shroff, D. J. Acosta, B. R. Alexander, H. O. Cole, Y. Zhang, N. A. Lynd, A. D. Ellington, H. S. Alper, Machine Learning-Aided Engineering of Hydrolases for PET Depolymerization. *Nature* **2022**, *604*, 662.
[23] R. Müller, H. Schrader, J. Profe, K. Dresler, W. Deckwer, Enzymatic Degradation of Poly(Ethylene Terephthalate): Rapid Hydrolyse Using a Hydrolase from T. Fusca. *Macromol. Rapid Commun.* **2005**, *26*, 1400.
[24] M. E. Sevilla, M. D. Garcia, Y. Perez-Castillo, V. Armijos-Jaramillo, S. Casado, K. Vizuete, A. Debut, L. Cerda-Mejía, Degradation of PET Bottles by an Engineered Ideonella Sakaiensis PETase. *Polymers* **2023**, *15*, 1779.
[25] A. N. Shirke, C. White, J. A. Englaender, A. Zwarycz, G. L. Butterfoss, R. J. Linhardt, R. A. Gross, Stabilizing Leaf and Branch Compost Cutinase (LCC) with Glycosylation: Mechanism and Effect on PET Hydrolysis. *Biochemistry* **2018**, *57*, 1190.
[26] C. Silva, S. Da, N. Silva, T. Matamá, R. Araújo, M. Martins, S. Chen, J. Chen, J. Wu, M. Casal, A. Cavaco-Paulo, Engineered Thermobifida Fusca Cutinase with Increased Activity on Polyester Substrates. *Biotechnol. J.* **2011**, *6*, 1230.
[27] C. Sonnendecker, J. Oeser, P. K. Richter, P. Hille, Z. Zhao, C. Fischer, H. Lippold, P. Blázquez-Sánchez, F. Engelberger, C. A. Ramírez-Sarmiento, T. Oeser, Y. Lihanova, R. Frank, H. G. Jahnke, S. Billig, B. Abel, N. Sträter, J. Matysik, W. Zimmermann, Low Carbon Footprint Recycling of Post-Consumer PET Plastic with a Metagenomic Polyester Hydrolase. *ChemSusChem* **2022**, *15*, e202101062.
[28] S. Kaabel, J. P. D. Therien, C. E. Deschênes, D. Duncan, T. Friščic, K. Auclair, Enzymatic Depolymerization of Highly Crystalline Polyethylene Terephthalate Enabled in Moist-Solid Reaction Mixtures. *Proc. Natl. Acad. Sci.* **2021**, *118*, 1.
[29] U. Abid, G. Sun, Y.-H. V. Soong, A. Williams, A. C. Chang, C. Ayafor, A. Patel, H.-W. Wong, M. J. Sobkowicz, D. Xie, Evaluation of Enzymatic Depolymerization of PET, PTT, and PBT Polyesters. *Biochem. Eng. J.* **2023**, *199*, 109074.
[30] R. P. Magalhães, J. M. Cunha, S. F. Sousa, Perspectives on the Role of Enzymatic Biocatalysis for the Degradation of Plastic PET. *Int. J. Mol. Sci.* **2021**, *22*, 11257.
[31] E. Marten, R.-J. Müller, W.-D. Deckwer, Studies on the Enzymatic Hydrolysis of Polyesters. II. Aliphatic–Aromatic Copolyesters. *Polym. Degrad. Stab.* **2005**, *88*, 371.
[32] S. W. Schubert, T. B. Thomsen, K. S. Clausen, A. Malmendal, C. J. Hunt, K. Borch, K. Jensen, J. Brask, A. S. Meyer, P. Westh, Relationships of Crystallinity and Reaction Rates for Enzymatic Degradation of Poly (Ethylene Terephthalate), PET. *ChemSusChem* **2024**, *17*, e202301752.
[33] T. B. Thomsen, T. S. Radmer, A. S. Meyer, Enzymatic Degradation of Poly(Ethylene Terephthalate) (PET): Identifying the Cause of the Hypersensitive Enzyme Kinetic Response to Increased PET Crystallinity. *Enzyme Microb. Technol.* **2024**, *173*, 110353.
[34] T. B. Thomsen, K. Almdal, A. S. Meyer, Significance of Poly(Ethylene Terephthalate) (PET) Substrate Crystallinity on Enzymatic Degradation. *New Biotechnol.* **2023**, *78*, 162.
[35] R. Wei, D. Breite, C. Song, D. Gräsing, T. Ploss, P. Hille, R. Schwerdtfeger, J. Matysik, A. Schulze, W. Zimmermann, Biocatalytic Degradation Efficiency of Postconsumer Polyethylene Terephthalate Packaging Determined by Their Polymer Microstructures. *Adv. Sci.* **2019**, *6*, 1900491.
[36] T. B. Thomsen, C. J. Hunt, A. S. Meyer, Influence of Substrate Crystallinity and Glass Transition Temperature on Enzymatic Degradation of Polyethylene Terephthalate (PET). *New Biotechnol.* **2022**, *69*, 28.
[37] V. Tournier, C. M. Topham, A. Gilles, B. David, C. Folgoas, E. Moya-Leclair, E. Kamionka, M.-L. Desrousseaux, H. Texier, S. Gavalda, M. Cot, E. Guémard, M. Dalibey, J. Nomme, G. Cioci, S. Barbe, M. Chateau, I. André, S. Duquesne, A. Marty, An Engineered PET Depolymerase to Break down and Recycle Plastic Bottles. *Nature* **2020**, *580*, 216.
[38] R. Androsch, A. M. Rhoades, I. Stolte, C. Schick, Density of Heterogeneous and Homogeneous Crystal Nuclei in Poly (Butylene Terephthalate). *Eur. Polym. J.* **2015**, *66*, 180.
[39] J. S. Blázquez, F. J. Romero, C. F. Conde, A. Conde, A Review of Different Models Derived from Classical Kolmogorov, Johnson and Mehl, and Avrami (KJMA) Theory to Recover Physical Meaning in Solid-State Transformations. *Phys. Status Solidi* **2022**, *259*, 2100524.
[40] A. Monshi, M. R. Foroughi, M. R. Monshi, Modified Scherrer Equation to Estimate More Accurately Nano-Crystallite Size Using XRD. *World J. Nano Sci. Eng.* **2012**, *02*, 154.
[41] C. Ślusarczyk, M. Sieradzka, J. Fabia, R. Fryczkowski, Supermolecular Structure of Poly(Butylene Terephthalate) Fibers Formed with the Addition of Reduced Graphene Oxide. *Polymers* **2020**, *12*, 1456.
[42] G. R. Strobl, M. Schneider, Direct Evaluation of the Electron Density Correlation Function of Partially Crystalline Polymers. *J. Polym. Sci. Polym. Phys. Ed.* **1980**, *18*, 1343.
[43] S. Weigert, P. Perez-Garcia, F. J. Gisdon, A. Gagsteiger, K. Schweinshaut, G. M. Ullmann, J. Chow, W. R. Streit, B. Höcker, Investigation of the Halophilic PET Hydrolase PET6 from Vibrio Gazogenes. *Protein Sci.* **2022**, *31*, 1.
[44] L. Avilan, B. R. Lichtenstein, G. König, M. Zahn, M. D. Allen, L. Oliveira, M. Clark, V. Bemmer, R. Graham, H. P. Austin, G. Dominick, C. W. Johnson, G. T. Beckham, J. E. McGeehan, A. R. Pickford, Concentration-Dependent Inhibition of Mesophilic PETases on Poly(Ethylene Terephthalate) Can Be Eliminated by Enzyme Engineering. *ChemSusChem* **2023**, *16*, 1.
[45] M. Ronkvist, W. Xie, W. Lu, R. A. Gross, Cutinase-Catalyzed Hydrolysis of Poly(Ethylene Terephthalate). *Macromolecules* **2009**, *42*, 5128.
[46] T. B. Thomsen, C. J. Hunt, A. S. Meyer, Standardized Method for Controlled Modification of Poly (Ethylene Terephthalate) (PET) Crystallinity for Assaying PET Degrading Enzymes. *MethodsX* **2022**, *9*, 101815.
[47] C. Bastioli, I. Guanella, G. Romano, Effects of Water Sorption on the Physical Properties of PET, PBT, and Their Long Fibers Composites. *Polym. Compos.* **1990**, *11*, 1.
[48] F. Dubelley, E. Planes, C. Bas, E. Pons, B. Yrieix, L. Flandin, Water Vapor Sorption Properties of Polyethylene Terephthalate over a Wide Range of Humidity and Temperature. *J. Phys. Chem. B* **2017**, *121*, 1953.
[49] D. Langevin, J. Grenet, J. M. Saiter, Moisture Sorption in Pet Influence on the Thermokinetic Parameters. *Eur. Polym. J.* **1994**, *30*, 339.
[50] M. J. PARKER, In *Comprehensive Composite Materials*; (Eds: A. Kelly, C. Zweben), Elsevier: Oxford, **2000**; pp 183–226.
[51] S. Weigert, B. Höcker, A. Gagsteiger, T. Menzel, A Versatile Assay Platform for Enzymatic Poly (Ethylene-Terephthalate) Degradation. *Protein Eng. Des. Sel.* **2021**, *34*, 1.
[52] K. H. Illers, Heat of Fusion and Specific Volume of Poly(Ethylene Terephthalate) and Poly(Butylene Terephthalate. *Colloid Polym. Sci.* **1980**, *258*, 117.
[53] M. Avrami, Kinetics of Phase Change. I General Theory. *J. Chem. Phys.* **1939**, *7*, 1103.
[54] M. Avrami, Kinetics of Phase Change. II Transformation - Time Relations for Random Distribution of Nuclei. *J. Chem. Phys.* **1940**, *8*, 212.

Manuscript received: August 13, 2025
Revised manuscript received: September 25, 2025
Version of record online: October 24, 2025